BBA - Biomembranes 1863 (2021) 183586

Contents lists available at ScienceDirect

BBA - Biomembranes

journal homepage: www.elsevier.com/locate/bbamem

Investigation of the domain line tension in asymmetric vesicles prepared via hemifusion

Thais A. Enoki [a,b,*], Joy Wu [a], Frederick A. Heberle [b], Gerald W. Feigenson [a]

[a] Department of Molecular Biology and Genetics, Cornell University, Ithaca, NY, United States of America
[b] Department of Chemistry, University of Tennessee, Knoxville, TN, United States of America

ARTICLE INFO

Keywords:
Asymmetric bilayers
Domain line tension
Coexistence of liquid disordered and liquid ordered phases
Asymmetric giant unilamellar vesicles
Hemifusion

ABSTRACT

The plasma membrane (PM) is asymmetric in lipid composition. The distinct and characteristic lipid compositions of the exoplasmic and cytoplasmic leaflets lead to different lipid-lipid interactions and physical-chemical properties in each leaflet. The exoplasmic leaflet possesses an intrinsic ability to form coexisting ordered and disordered fluid domains, whereas the cytoplasmic leaflet seems to form a single fluid phase. To better understand the interleaflet interactions that influence domains, we compared asymmetric model membranes that capture salient properties of the PM with simpler symmetric membranes. Using asymmetric giant unilamellar vesicles (aGUVs) prepared by hemifusion with a supported lipid bilayer, we investigate the domain line tension that characterizes the behavior of coexisting ordered + disordered domains. The line tension can be related to the contact perimeter of the different phases. Compared to macroscopic phase separation, the appearance of modulated phases was found to be a robust indicator of a decrease in domain line tension. Symmetric GUVs of 1,2-distearoyl-sn-glycero-3-phosphocholine (DSPC)/1,2-dioleoyl-sn-glycero-3-phosphocholine (DOPC)/1-palmitoyl-2-oleoyl-glycero-3-phosphocholine (POPC)/cholesterol (chol) were formed into aGUVs by replacing the GUV outer leaflet with DOPC/chol = 0.8/0.2 in order to create a cytoplasmic leaflet model. These aGUVs revealed lower line tension for the ordered + disordered domains of the exoplasmic model leaflet.

1. Introduction

The plasma membrane (PM) exhibits important and vital properties for cell function such as protein sorting, signaling, and transduction. The lipid bilayer of the PM has a variety of lipid types, including different melting points: saturated and unsaturated acyl-chains, lipids with different head groups and intrinsic curvatures, and cholesterol (chol). In addition, the exoplasmic leaflet, which faces the exterior of the cell, has a different lipid composition from the cytoplasmic leaflet, which faces the cell interior. These differences in lipid composition could drive fundamental lipid-lipid interactions, leading to different physical-chemical properties of each individual leaflet. For example, the lipid composition of the exoplasmic leaflet is enriched in sphingomyelin (SM) and low-melting phosphatidyl choline (PC). Simplified model membranes prepared in vitro, e.g. brain SM (bSM)/DOPC/chol, exhibit coexistence of liquid phases, liquid disordered (Ld) + liquid ordered (Lo). Similarly, when the high melting lipid bSM is replaced by a high-melting PC such as DSPC, the ternary mixture also exhibits coexisting Ld + Lo domains. On the other hand, the cytoplasmic leaflet lacks high melting lipids, lipids with long saturated hydrocarbon chains, and its composition includes a large fraction of polyunsaturated lipids, lipids with very low melting points [1,2]. Therefore, due to the near absence of high-melting lipids in the cytoplasmic leaflet, it is found that models of this leaflet form a single fluid phase. Additionally, the cytoplasmic leaflet has large fractions of phosphatidylethanolamine (PE) and phosphatidylserine (PS). These lipids could increase the complexity of the properties of the PM cytoplasmic leaflet, where PE exhibits a negative intrinsic curvature [3], and negatively charged PS adds an additional electrostatic contribution to the interactions present in this leaflet.

Numerous questions about intra- and interleaflet interactions are raised regarding the bilayer asymmetry, including the peculiarities of individual leaflets. Does the phase-separated leaflet induce domains in the otherwise uniformly fluid leaflet? Does the fluid leaflet modify or even abolish the phase separation on the apposed leaflet? Increasingly, asymmetric model membranes have been used to investigate interleaflet interactions to better understand the coupling between leaflets [4,5].

Theoretical models have explored coupling between leaflets [4,5]. Experimentally, a few methods can produce asymmetric bilayers

* Corresponding author at: Department of Molecular Biology and Genetics, Cornell University, Ithaca, NY, United States of America.
E-mail address: ta327@cornell.edu (T.A. Enoki).

https://doi.org/10.1016/j.bbamem.2021.183586
Received 30 September 2020; Received in revised form 28 January 2021; Accepted 12 February 2021
Available online 26 February 2021

[6–10]. For the investigation of interleaflet coupling, it is important to use a method free of residual organic solvent that could potentially accumulate at the bilayer midplane. Especially useful for this purpose is a method for exchanging the outer leaflet lipids of vesicles using cyclodextrin (CD) [11]. And as we discuss here, the hemifusion between giant unilamellar vesicles (GUVs) and a supported lipid bilayer (SLB) [7] creates a floating asymmetric model bilayer, an aGUV.

The coupling between the inner and the outer leaflet can be discussed in terms of how one leaflet affects the properties of the other leaflet. For example, Chiantia and London monitored the diffusion coefficient of fluorescent lipid probes in the inner and the outer leaflet of aGUVs prepared by CD exchange [11]. In their series of experiments, the inner leaflet of aGUVs has different low-melting (low-Tm) lipids, and the outer leaflet has high-melting (high-Tm) lipids such as sphingomyelins from brain or milk. The authors measured slower diffusion in both aGUV leaflets, suggesting that SM lipids increase the physical interaction (and hence the coupling) between leaflets via interdigitation of their long N-acyl chains. This finding was further supported by the especially prominent reduction in diffusion for aGUVs containing milk SM, which is rich in C22:0, C23:0, and C24:0-SM species.

Heberle et al. studied asymmetric large unilamellar vesicles (aLUVs) prepared using CD-mediated exchange, and investigated how one fluid leaflet composed of POPC interacts with the apposed leaflet of POPC/DPPC using small-angle neutron scattering (SANS) [12]. Their results showed no change in the packing density of POPC in the inner leaflet, whereas the DPPC-rich domains in the outer leaflet showed a reduced packing density due to the coupling of the opposed POPC leaflet [12]. Eicher et al. reported that the lipid intrinsic curvature may also play a role in interleaflet interactions. In DSC experiments of aLUVs prepared using CD exchange, a significant difference was observed between the thermograms for asymmetric vesicles with POPE in the inner leaflet and POPC in the outer leaflet, or the reverse bilayer (POPC in the inner leaflet and POPE in the outer leaflet) [13].

In other work from London's group, the thermal stability of Ld and Lo domains in asymmetric vesicles was studied by monitoring the FRET signal of fluorescent probes [14,15]. Wang and London [14] studied asymmetric vesicles in which one leaflet is phase-separated and the other enriched in the fluid lipid DOPC. They used different mixtures for the phase-separated leaflet in which the high-Tm lipids have different chain lengths. When the high-Tm lipid is DSPC, the existence of domains as a function of temperature is similar to what is observed for symmetric vesicles. On the other hand, when the high-Tm lipid is DPPC, the asymmetric bilayer becomes uniform at a lower temperature compared to the symmetric vesicles [14]. This result implies different interleaflet coupling for these different mixtures. However, without a clear measurement of coupling, it is also possible that another competing interaction, such as the line tension, is playing an important role in the domain behavior of asymmetric bilayers.

In symmetric vesicles, line tension controls domain size and morphology [16]. Line tension is the extra energy per unit of length along interface between the Ld and the Lo phases. For phase-separated lipid mixtures with high line tension, the coexisting domains coalesce into large round domains, which minimizes the contact perimeter between two phases. For sufficiently lower line tension, the contact perimeter between the Ld and the Lo phases increases, leading to irregularly-shaped domains that form stripes and other patterns. Coexisting domains with these features are called modulated phases. For even lower line tension, the total perimeter between the Ld and the Lo phases greatly increases, splitting the domains into many tens of nanometer-scale domains. From the experimental point of view, the sizes of these nanodomains are below the optical resolution [17–23], but they can be observed with cryogenic electron microscopy [24]. In summary, the progress of domain morphologies in GUVs (large domains, modulated phases and uniform appearance/nanodomains) is directly related to the domain line tension.

In previous work, we systematically studied the range of lipid composition where modulated phases are observed for 12 different lipid mixtures [16]. In this previous work, we studied lipid mixtures that model the plasma membrane exoplasmic leaflet by use of four lipid components generally described as high melting (high-Tm) lipid/low melting (low-Tm) lipid-1/low-Tm lipid-2/chol. The low-Tm lipids differ from each other in length and unsaturation of their hydrocarbon chains, and melting points. A prominent example of such a mixture is DSPC/DOPC/POPC/chol. Note that the ternary mixture DSPC/DOPC/chol forms macrodomains, with visible micron-sized domains on an optical microscope, whereas GUVs prepared with the ternary mixture DSPC/POPC/chol exhibit a uniform appearance. In addition, we showed that DSPC/POPC/chol forms domains of sizes of the order of tens of nanometers, and therefore the domain sizes are below optical resolution [17–23]. The observation of nanodomains was further confirmed by different research groups using a variety of experimental techniques [25,26]. Interestingly, for the four-component mixture that combines the two low-Tm lipids mentioned above, the modulated phases are observed over a specific and narrow compositional range, here called a ρ-window [21]. The appearance of modulated phases indicates a lower Ld/Lo line tension compared to round and macroscopic domains.

The method used in these studies is simple, based on the observation and comparison of domain morphologies. We prepare and observe a compositional trajectory of samples with different lipid compositions. Importantly for this method, the ratios of high-Tm/(low-Tm-1 + low-Tm-2)/chol are fixed. Therefore, the variation of the lipid composition depends only on the fractions of the two low-Tm lipids. To facilitate the comparison between different lipid mixtures, we use a single parameter, ρ, as previously reported [21]. For mixtures composed of DOPC and POPC, ρ is given by

$$\rho = \frac{\chi_{DOPC}}{\chi_{DOPC} + \chi_{POPC}} \quad (1)$$

where χ_{DOPC} and χ_{POPC} represent the fraction of DOPC and POPC, respectively (for more details see Fig. 1).

As examples of our previous observations, we can compare three different lipid mixtures and the lipid composition at the center of their ρ-window, where each mixture forms modulated phases. For example, modulated phases are observed for DSPC/DOPC/POPC/chol = 0.39/0.04/0.35/0.22 (ρ = 0.3), pSM/DOPC/POPC/chol = 0.39/0.12/0.27/0.22 (ρ = 0.1) and bSM/DOPC/POPC/chol = 0.39/0.31/0.08/0.22 (ρ = 0.6), where lower values of ρ indicate smaller fractions of DOPC and larger fractions of POPC. The replacement of DOPC by POPC lowers the domain line tension. The comparison of these three different lipid mixtures shows that the mixture with lower ρ need a higher fraction of POPC to lower the domain line tension sufficiently to form modulated phases. These observations imply that we can qualitatively compare the domain line tension by use of an optical microscope. For these mixtures, the line tension increases in the order bSM/DOPC/POPC/chol < DSPC DOPC/POPC/chol < pSM DOPC/POPC/chol. To demonstrate that this observation is correct, we measured the domain line tension of these mixtures using flicker spectroscopy, as previously reported [16]. For ρ = 1, i.e. in the absence of POPC, the mixtures containing the high-Tm lipid bSM, DSPC or pSM, have values of line tension 1.2, 1.4, and 2.7 pN, respectively [16]. It should be noted that the observed difference in line tension does not necessary depend on the increasing fraction of POPC. In the example above, the flicker spectroscopy measurements were performed in ternary mixtures without POPC described as high-Tm lipid/DOPC/chol. Therefore, the line tension depends on the lipid-lipid interactions in the Ld and the Lo phase of each mixture. However, the first method presented here makes use of the variation of POPC fraction, i.e. varying ρ, to investigate the compositional range where modulated phases are observed. Thus, as we have previously shown, the investigation of modulated phases for varying ρ is a simple and robust method that can be used to control changes in line tension between different lipid mixtures. For these observations, a shift in the appearance of

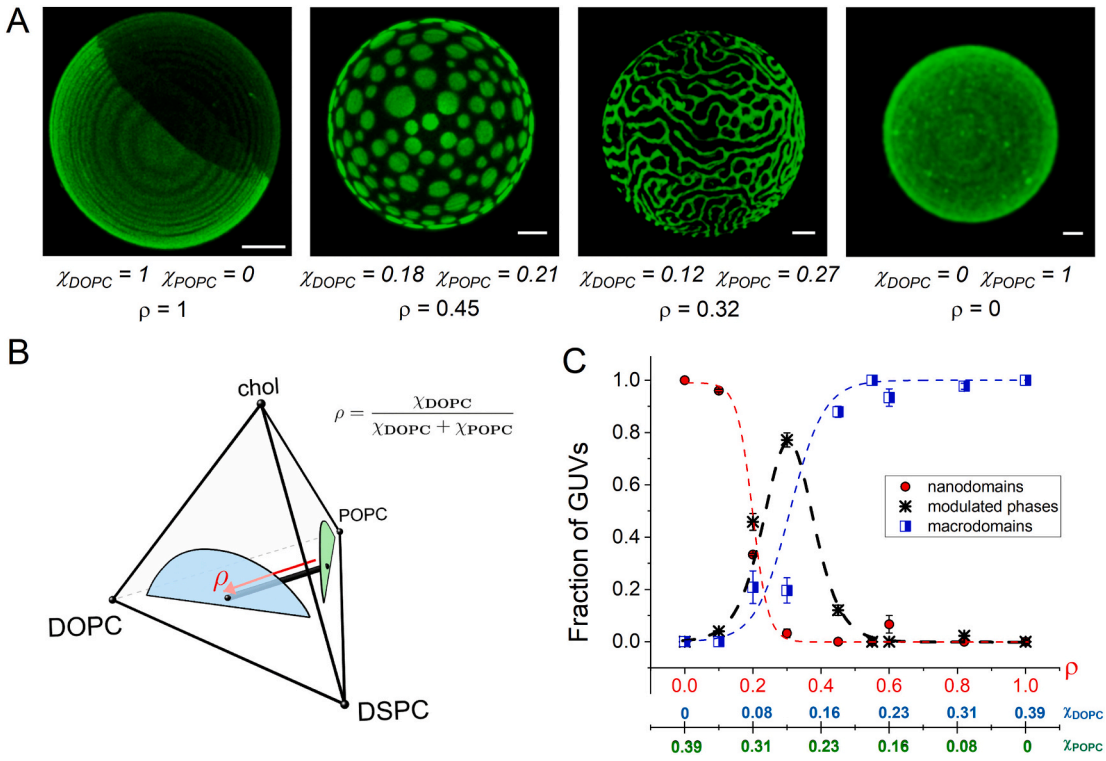

Fig. 1. Phase morphologies are controlled by lipid composition. (A) GUV images show different phase morphologies at room temperature, from left to right (scale bars = 5 μm): macrodomains that coalesce in a single or a few large domains (ρ = 1); broken macrodomains (ρ = 0.45); phase-modulated domains (ρ = 0.32); and uniform appearance (ρ = 0). (B) The partial quaternary phase diagram of the DSPC/DOPC/POPC/chol mixture, shown as a tetrahedron. The shaded regions correspond to Ld + Lo regions in the room-temperature ternary phase diagrams of DSPC/DOPC/chol (near-left face) and DSPC/POPC/chol (far-right face). The lipid composition of the GUVs shown in (A) is tuned by different fractions of DOPC and POPC, as described by ρ. (C) A plot of the fraction of GUVs vs. composition that exhibit nanodomains, phase modulated domains and macrodomains as indicated in the legend. For DSPC/DOPC/POPC/chol a majority of the GUVs exhibit modulated phases at ρ ~ 0.3 (ρ-window center). Errors are calculated from the standard deviation (n = 17–32 per composition).

modulated phases to higher values of ρ implies a relatively lower line tension.

As explained in more detail later, because of experimental limitations the use of flicker spectroscopy to measure line tension is not practical for aGUVs. Instead, the systematic study of the appearance by use of optical microscopy of modulated phases with ρ values can be used to investigate and compare the domain line tension in both symmetric and aGUVs.

Here, we present a systematic study of the symmetric four-component system, DSPC/DOPC/POPC/chol, varying the fractions of DOPC and POPC, i.e. ρ, in order to investigate the appearance of modulated phases. Then we compare the symmetric modulated phase appearance to that of aGUVs as a function of their lipid composition. Here, aGUVs are prepared via hemifusion [7]. To better control the changes in the outer leaflet composition, we assemble a single fluid phase that models the PM cytoplasmic leaflet, as an aGUV outer leaflet, whereas the aGUV inner leaflet has lipid composition that phase separates into Ld + Lo domains to model the PM exoplasmic leaflet. Thus, we prepared a series of aGUVs with the inner leaflet having different lipid composition, where the fractions of DOPC and POPC are varied, whereas the outer leaflet of all samples is replaced by DOPC/chol = 0.8/0.2. This study enables inferring the changes in domain line tension in asymmetric compared to symmetric bilayers. We found that asymmetric domains in these kinds of bilayers have a lower line tension compared to symmetric Ld + Lo domains.

2. Materials and methods

2.1. Chemicals

DSPC (1,2-distearoyl-*sn*-glycero-3-phosphocholine), DOPC (1,2-dioleoyl-*sn*-glycero-3-phosphocholine) and POPC (1-palmitoyl-2-oleoyl-*sn*-glycero-3-phosphocholine) were from Avanti Polar Lipids (Alabaster, AL, USA); cholesterol (Chol) from Nu Chek Prep (Elysian, MN, USA); HEPES (4-(2-hydroxyethyl)-1-piperazineethanesulfonic acid), NaCl (sodium chloride), $CaCl_2$ (calcium chloride) and EDTA (ethylenediaminetetraacetic acid) from Sigma-Aldrich (St. Louis, MO, USA). We performed thin-layer chromatography (TLC) using ~20 μg of lipid diluted in chloroform to examine the purity of lipids, which was found to be >99%. Briefly, lipids were spotted onto prewashed, activated silica gel GHL plates (Analtech, Newark, DE, USA). Plates were developed with chloroform/methanol/water (65/25/4). Chol stock purity was checked with TLC in petroleum ether/diethyl ether/chloroform (7/3/3). Phospholipid concentration was determined to <1% error using inorganic phosphate assay [27]. Fluorescent dyes were TopFluor-PC, here named TFPC (1-palmitoyl-2-(dipyrromethaneboron difluoride) undecanoyl-sn-glycero-3-phosphocholine) from Avanti Polar Lipids (Alabaster, AL, USA); DiD (1,1′-dioctadecyl-3,3,3′,3′-tetramethylindodicarbocyanine perchlorate) and DiI (1,1′-didodecyl-3,3,3′,3′-tetramethylindocarbocyanine perchlorate) from ThermoFisher scientific (Molecular probes) (Waltham, MA, USA). Dyes were prepared as stock solutions in chloroform. We used the absorbance of the fluorescent dyes in order to measure the dye concentration. For DiI, DiD and TFPC we used molar extinction coefficients ε = 144,000, 91,800 and 270,000 $(M{\cdot}cm)^{-1}$, respectively. TLC also confirmed >99% purity of the dye stocks.

2.2. Preparing SUVs for lipid deposition of the supported bilayer

Rapid Solvent Exchange [28] was used to prepare liposomes (~2.5 mM total lipid concentration, ~500 μL total volume) containing the lipid fluorophore TFPC at a 1/1500 dye/lipid ratio. The liposomes were prepared in glass test tubes (13 × 100 mm) with screw caps, which were then placed in the center of a circular bath sonicator (Sonblater, Narda ultrasonic corporation, NY) for ~20 min. Samples were turbid prior to sonication and translucent after sonication, as previously described [7].

2.3. Cleaning the chambers for supported lipid bilayers

Supported lipid bilayers (SLB) were prepared in Lab-Tek II chambered cover glass dishes (Thermo Fisher Scientific 155382) having 4 wells of size 1 × 2 cm. SLBs were assembled on the cover slides of these dishes. The cover slide of each well was washed with a freshly prepared solution of ~1 M KOH (Sigma-Aldrich) in ethanol by dripping the KOH solution into each well directly onto the top of the cover slide. After 20 min, the chamber was rinsed thoroughly with Milli-Q water (Thermo Fisher Scientific). The excess water in the chamber was first air-dried, then further dried with a flow of N_2. Finally, the chamber was cleaned in a plasma cleaner/sterilizer (model PDC-3 G, Harrick Plasma, Ithaca, NY) for 2 min.

2.4. Deposition and observation of one supported bilayer

After the dish was removed from the plasma cleaner, 500 μL of the SUV dispersion was mixed with 1 M NaCl 1:1 by volume and dispensed onto the cover slide of each chamber. The lipid dispersion quickly spread over the freshly-cleaned cover glass, covering its entire surface. The chambers were then kept at 4 °C for 2 h. Then, the dish with total volume of 2 mL per chamber was immersed in Milli-Q water (2 L). The SLBs were gently rinsed with water using a 20 mL syringe to remove any lipid aggregates loosely attached to the SLB surface. After sufficient rinsing (as judged by examination of the SLB with a fluorescence microscope, followed by further water rinsing as necessary) the Milli-Q water in the chamber was replaced by buffer (HEPES 25 mM, NaCl 35 mM, pH = 7.43, ~103 mOsm) with an osmolarity matching that of the aqueous sucrose used to prepare GUVs. The osmolality of buffers and solutions used in this work was measured using an osmometer (Model 5004, Precision Systems, Inc., Natick, MA).

2.5. GUV preparation

GUVs were prepared using the electroformation procedure [29]. Briefly, lipids and dyes dissolved in chloroform were spread on microscope slides coated with ITO (indium tin oxide) at 40 °C. Samples were kept under vacuum of (~ 0.15 Torr) for 2 h using a heated desiccator (HeatVac, Minneapolis, MN) attached to a vacuum pump with temperature set to 50 °C. ITO slides were sealed with Buna-N O-rings to create a chamber, and the lipid film then hydrated with ~100 mM sucrose. GUVs were formed at 50 °C by electroswelling under an applied voltage of 1 V peak-to-peak at 5 Hz for 2 h. Then GUVs were slowly cooled from 50 °C to 23 °C over 12 h. We also tested a slower cooling rate of 20 h over the same temperature range to confirm that 12 h was slow enough to establish equilibrium for these liquid systems. Here the word equilibrium is only applied to symmetric GUVs for which we know the phase diagrams and the tielines of the two phase region. For composition along the same tieline, equilibrium implies that a certain lipid has the same chemical potential in the Ld phase or in the Lo phase. The reproducibility of domain morphologies to repeated heating and cooling cycles was also examined: after each cycle, we observed that GUVs displayed the same domain morphology according to their lipid composition. GUVs at 23 °C were collected in Eppendorf tubes and added to the SLB chambers as described below. For aGUV preparation via hemifusion, we initially prepared symmetric GUVs labeled with DiD (1/2500 dye/lipid). For line tension measurements of symmetric GUVs, we used DiI (1/500 dye/lipid).

2.6. GUV and SLB hemifusion

A small aliquot (15–20 μL) of symmetric GUVs was collected using a pipettor with a large orifice tip (VWR International, Radnor, PA) and dispensed inside the SLB chamber filled with 1.0 mL of HEPES buffer. Smaller aliquots (3–5 μL) of these GUVs were dropped over the SLB, settling onto the SLB. Then, 5 μL aliquots of Ca^{2+} at 20 mM were added to the SLB chamber. After 20–30 min, EDTA at 6 mM was added to chelate Ca^{2+} to prevent further fusion. To harvest the hemifused aGUVs attached to the SLB, a 1000 μL pipettor with a large orifice tip was used, gently pipetting ~200 μL up and down holding the pipet tip about 0.2 cm from the chamber bottom. This procedure shears the GUVs off the supported bilayer. aGUVs were then placed in a different chamber or slide for study. The Ca^{2+} concentration of all buffers and samples in this work was measured using the fluorescent indicator dye for Ca^{2+}, Rhod-5N (Invitrogen). Rhod-5N is sensitive in the range of ~0.1–10 mM Ca^{2+}. We prepared a calibration curve from a buffer by use of a Ca^{2+} standard solution of concentration 1.00 M (J.T. Baker Chemical Co.). For more details, see our previous report. [7].

Although, Ca^{2+} and EDTA are only on the exterior of the vesicles, it is important to note that we adjusted the osmotic pressure inside and outside the vesicles studied here (control GUVs and aGUVs). In our symmetric GUVs controls in the presence of Ca^{2+} and EDTA we do not observe changes in the domain morphology, for example vanishing domains when the lipid composition should form domains, nor creating domains when the lipid composition should form uniform bilayers. These observations can be found in the Supporting material. Because differences in osmolarity can indeed cause changes in the domain morphologies, we used freshly prepared <1–2 weeks old buffers and solutions, and measured the osmolarity of these solutions in every preparation.

2.7. aGUV analyses: measuring the percentage of lipid exchange

We used the fluorescence intensity of labeled GUVs and aGUVs to calculate the percentage of lipid exchange as follows. After hemifusion and exchange, unsupported aGUVs contain two types of fluorophore: DiD (fluorescence emission peak λ_{em} = 644 nm, far red) that was initially incorporated into the GUVs, and TFPC (fluorescence emission peak λ_{em} = 496 nm, green) initially incorporated into the SLB. DiD and TFPC were excited with laser lines at 488 nm and 640 nm, respectively; the emission spectra are sufficiently far apart that there is negligible cross talk between the red and green microscope channels. After hemifusion, the inner leaflet of aGUVs is labeled only with DiD, while the outer leaflet contains a mixture of DiD and TFPC that depends on the level of exchange. For aGUVs that achieved <100% exchange, some residual DiD will be found in the aGUV outer leaflet. On the other hand, TFPC will be located exclusively in the aGUV outer leaflet. As previously reported, we compare the measured dye intensities in aGUVs to measurements in symmetric GUVs, which act as controls that were not subjected to hemifusion. After lipid and dye exchange between the GUV and SLB, the fluorescence of DiD and TFPC will be some fraction of the intensity measured in symmetric GUVs, and these fractions are used to independently calculate the percentage of lipid exchange.

To measure the dye intensity ratio GUV/aGUV, we used a built-in ImageJ (Fiji) routine that draws 360 line scans crossing the GUV or aGUV edge. Using a built-in Mathematica function (v11.0, Wolfram Research, Champaign, IL) we measured the peak intensity of each profile and plotted it as a function of the polar angle θ (see Fig. 4). The signal was integrated as a function of θ in order to measure the total intensity for each GUV or aGUV micrograph (see Figs. 4 and 5). The total intensity of aGUVs and symmetric GUV controls was then compared as shown in the example of Fig. 5. Fig. 6 plots the correlation between the percentage

of exchange calculated from each dye independently [i.e., Exchange, DiD (%) vs. Exchange, TFPC (%)], where we use aGUVs that achieved the selection criterion of agreement between the independent analyses of both dyes. Cases in which the calculated percentage of lipid exchange for DiD and TFPC do not agree occur for multilamellar vesicles, for example.

2.8. Line tension measurements

Line tension was measured using the flicker spectroscopy method of Esposito et al. [30]. The fluctuation spectrum of a phase domain boundary on a GUV is decomposed into Fourier modes that are related to line tension by

$$\langle |u_n|^2 \rangle = \frac{2k_BT}{\sigma\pi R_d(n^2-1)}, \quad (2)$$

where n is the mode number, u_n is the mode amplitude, R_d is the radius of a circle yielding the domain area, k_B is the Boltzmann constant, T is the absolute temperature, and σ is the line tension [30]. As previously reported, line tension obtained from domain fluctuations does not depend on the nature of the domain or the surrounding phases, i.e. either Ld or Lo domains yield similar line tension values. In addition, for sufficiently large GUVs ($R \gg R_d$), vesicle size does not influence these measurements. Here, we chose GUVs with $R > 20$ μm and $R_d \approx 2.5$ μm.

2.9. Line tension data collection and analysis

For line tension measurements, we prepared microscope slides using 2–5 μL of GUV samples. GUV samples were sealed using a coverslip No. 1.5 and a traditional microscope slide with a silicone spacer of 0.25 mm thickness (Sigma-Aldrich). GUVs for line tension measurements were prepared with a higher dye concentration of DiI (1/500 dye/lipid) in order to achieve the required contrast. We made a substantial effort to avoid light-induced artifacts, preparing and keeping in the dark and using minimal room illumination during data acquisition. To find domains that were right on top of the GUV and of appropriate size, we searched the sample field using fluorescence at 2% of illumination intensity of the Spectra X light source. Once the domain qualifications were satisfied, data were collected at 50% illumination intensity. During the acquisition, the Spectra X was triggered by the camera so that the LED was only on during the 10 ms exposure time. During the 20 ms between frames, the LED was off.

To facilitate the search for domains of diameter approximately 5 μm and on the top of the GUV, the GUV samples were heated above the melting point of the high melting lipid, ~50 °C. Then, 2–5 μL of GUV was collected and placed in a microscope slide and sealed with a cover slide, as described above. The microscope slide was then placed on the lab bench, at room temperature of 21 °C, or else in contact to dry ice for a few seconds. Because of the small volume of the sample on the microscope slide, the sample quickly went to room temperature. This procedure made it easier to find small domains on top of GUVs.

Line tension measurements were performed using an inverted Nikon Eclipse TI-E (Nikon Instruments) with a 60 × 1.2 NA water immersion objective and an additional 1.5× intermediate magnifier for a total magnification of 90× and corresponding pixel size of ~71 nm for images acquired with a Zyla 5.5 sCMOS camera (Andor Technology Ltd). Excitation of DiI was via a Spectra X Light Engine (Lumencor, Inc.) with an LED (Wavelength/bandwidth 542 nm/27 nm). Filters in the excitation and emission pathways were 545 nm/25 nm and 605 nm/70 nm, respectively. Data acquisition and control of illumination intensity were performed using the software NIS-Elements Basic Research (MVI, Inc.). Analysis of domain fluctuations was implemented using MATLAB v.2010a (Mathworks, Natick, MA) following the basic methodology of Baumgart et al. [30], as previously reported [16]. Importantly, we checked the line tension measurements for every successive subset of 100 frames. Any abrupt change in these subsets can indicate light-induced artifacts, and such data were discarded from our analyses. Light-induced artifacts can also lead to irregular domain shapes, and these cases are also not considered in our analyses. For more details, see Supporting material and our previous paper [16].

3. Results and discussion

We investigated the Ld/Lo line tension by visualizing the domain phase morphologies in GUVs or aGUVs. First, we describe the correlation between domain morphology and domain line tension in symmetric GUVs. Then we show the results obtained for aGUVs, focusing on how the percentage of lipid exchange changes the bilayer properties. For aGUVs having a percentage of lipid exchange > 60%, we compare the domain morphologies and line tension values of aGUVs with those of symmetric GUVs.

3.1. Domain morphology is correlated with line tension in GUVs

GUVs composed of the ternary mixture DSPC/DOPC/chol = 0.39/0.39/0.22 form micron-sized domains (here called “macrodomains”) in GUVs, as shown in Fig. 1A. The Ld + Lo phase separation is characterized by large domains and a line tension of ~1.4 pN, as we previously measured (4) and discuss below. This high line tension imposes a large energy cost to form domain interface. A single large domain minimizes the perimeter between the Ld and the Lo phases, and hence minimizes the total unfavorable boundary energy. In this work, the line tension was controlled by varying the value of ρ, our metric to quantify the ratio of DOPC to the total low-melting lipid (defined in Eq. (1)). The three-component mixture DSPC/POPC/chol corresponds to ρ = 0, the three-component mixture DSPC/DOPC/chol corresponds to ρ = 1, and any quaternary mixture of DSPC/DOPC/POPC/chol corresponds to a value $0 < \rho < 1$. Decreasing ρ—that is, increasing the fraction of POPC and decreasing the fraction of DOPC—decreases the line tension and modifies the domain morphology.

The sequence of images in Fig. 1A shows symmetric GUVs prepared at different values of ρ. As ρ decreases, the domain morphology changes from one or two large domains ($\rho > 0.5$), to macrodomains broken into large domains that are surrounded by a continuous phase ($0.5 > \rho > 0.35$), to domains shaped in patterns termed modulated phases ($0.35 > \rho > 0.2$), and GUVs with a uniform appearance ($\rho < 0.2$). For this sequence of images, we observe that the transition from macrodomains to modulated phases is accompanied by a gradual increase of the total perimeter of Ld and Lo phase contact, implying that the energy cost in the domain interface (and therefore the Ld/Lo line tension) decreased. For GUVs composed of DSPC/POPC/chol = 0.39/0.39/0.22 (i.e., ρ = 0) which display a uniform appearance by light microscopy, we previously reported the existence of Ld + Lo nanodomains [18,19,22,23,31]. The same trend discussed above applies to nanodomains, where in this case a larger number of domains with much smaller sizes are formed, leading to a larger total perimeter of two phases in contact.

Fig. 1B shows a partial phase diagram for DSPC/DOPC/POPC/chol [31]. Ternary phase diagrams for DSPC/DOPC/chol and DSPC/DOPC/chol are shown on the far-left and far-right faces of the tetrahedron, respectively, and were previously determined by FRET experiments [31]. The red arrow marks the lipid compositional trajectory used in this work, and shows the variation of the fractions of DOPC and POPC with increasing ρ. The fractions of high-melting lipid DSPC and chol remain constant along these trajectories, such that the phase mole fractions hardly change (i.e., $\chi_{Ld} \approx \chi_{Lo} \approx 0.5$ along the arrow in Fig. 1B). Because the phase fractions are approximately equal, changes in the domain morphology do not involve one phase becoming the minority phase surrounded by a higher fraction of the second phase. In addition, changes in the domain morphologies are not induced by mechanical stress (such as deflating or inflating the GUVs) in this work, because we maintained the same osmotic pressure inside and outside the GUVs. We

also minimized light-induced artifacts that can occur when high dye concentrations combined with long light exposure results in dye cross-linking, which in turn can induce domain formation and/or affect domain morphologies such as modulated phases [32]. Here, we used very low dye concentration (lipid/TFPC = 1/1500 = 0.06 mol% and lipid/DiD = 1/2500 = 0.04 mol% - see Materials and methods).

Modulated phases occur in GUVs at sufficiently low line tension. We refer to the compositional range where this low line tension occurs as the "ρ-window" [21]. Fig. 1C illustrates the ρ-window for DSPC/DOPC/POPC/chol, which is centered at ρ = 0.32. The ρ-window marks a key domain size transition, from nanodomains to macrodomains, as previously reported [16]. Thus, for lipid composition with ρ values below the ρ-window, GUVs have a uniform appearance, and for compositions above the ρ-window GUVs show macrodomains. Fig. 1C shows the fractions of GUVs with nanodomains, modulated phases and macrodomains as a function of ρ, with fractions of DOPC and POPC also shown. These data confirm our previous findings [16] and extend them with the observation that the ρ-window is independent of the choice of dye used to label the Ld phase: we found an identical ρ-window for DSPC/DOPC/POPC/chol using DiD, TFPC and DiI (see Figs. 1, 2 and 8).

In order to demonstrate that observation of domain morphologies can be used to visually indicate the Ld/Lo line tension, we measured the line tension using flicker spectroscopy as developed by Baumgart's group and collaborators [30,33]. Fig. 2 shows the Ld/Lo line tension for different domain morphologies.

We tested the reproducibility of domain morphologies for GUVs showing either macrodomains (Fig. 2A, upper image) or modulated phases (Fig. 2A, lower image). These samples were heated above the melting point of the high melting lipid (50 °C) and then slowly cooled at ~2 °C/h to room temperature to reach thermodynamic equilibrium. To verify the reproducibility of these domains, we heated and cooled GUVs with macrodomains or modulated phases a few times, collecting images between the heating and cooling cycles. We observed the same domain morphology after each heating/cooling cycle, with macrodomains or modulated phases appearing according to mixture composition (see Data in Brief co-submission).

To measure domain fluctuations, we used a previously reported strategy [16] of heating the GUVs above the melting point of the high melting lipid, then quickly cooling to room temperature, resulting in kinetically trapped small domains. We then monitored the domain fluctuations for samples with different ρ values and calculated the domain line tension using Eq. (2). Fig. 2B shows the measured line tension for GUVs with different lipid composition.

When these samples were heated and slowly cooled to room temperature, the GUVs recovered their phase morphologies as shown in Fig. 2B images. Fig. 2B clearly shows that the domain morphology is correlated with line tension: the line tension decreases significantly from σ = 1.4 ± 0.2 pN at ρ = 1 (where macrodomains are observed) to σ = 0.56 ± 0.05 pN at ρ = 0.32 (where modulated phases are observed). Therefore, the domain morphologies observed in GUVs can be used to infer the Ld/Lo line tension.

For investigating line tension in aGUVs, we chose the simpler, qualitative method described above (i.e., visual inspection of domain morphologies) rather than performing flicker measurements. This choice was made primarily because domains that satisfy flicker spectroscopy criteria for tracking fluctuations (namely, domains of ~5 μm diameter positioned directly on top of the GUV, and much smaller than the GUV size to avoid effects of domain curvature) are relatively rare. Taken together with the challenge of successful aGUV preparation by hemifusion, the morphology-based method enabled comparisons between symmetric and asymmetric GUVs that would otherwise have not been possible. We next describe the results obtained for aGUVs, and further we compare the ρ-window of symmetric GUVs and aGUVs.

3.2. Hemifusion yields aGUVs

To facilitate the ensuing discussion, we briefly illustrate the procedure for preparing aGUVs via hemifusion [7] in Fig. 3. SLBs were prepared by depositing SUVs on the cover slide of a chamber dish, and GUVs were prepared using the electroformation procedure. We used different fluorescent probes to label the GUVs and the SLB. We added symmetric GUVs to the SLB chamber, and monitored the contact between them using a confocal microscope. At this point, GUVs and SLB contain only their original fluorescent dye. After adding the fusogenic agent Ca^{2+} to the chamber, we observed dye exchange between the GUVs and the SLB. Hemifusion precedes the full fusion event [34–38] and consists of the fusion of only the outer leaflets of the GUV and the SLB. Hence both outer leaflets are connected, and lipids and dyes freely

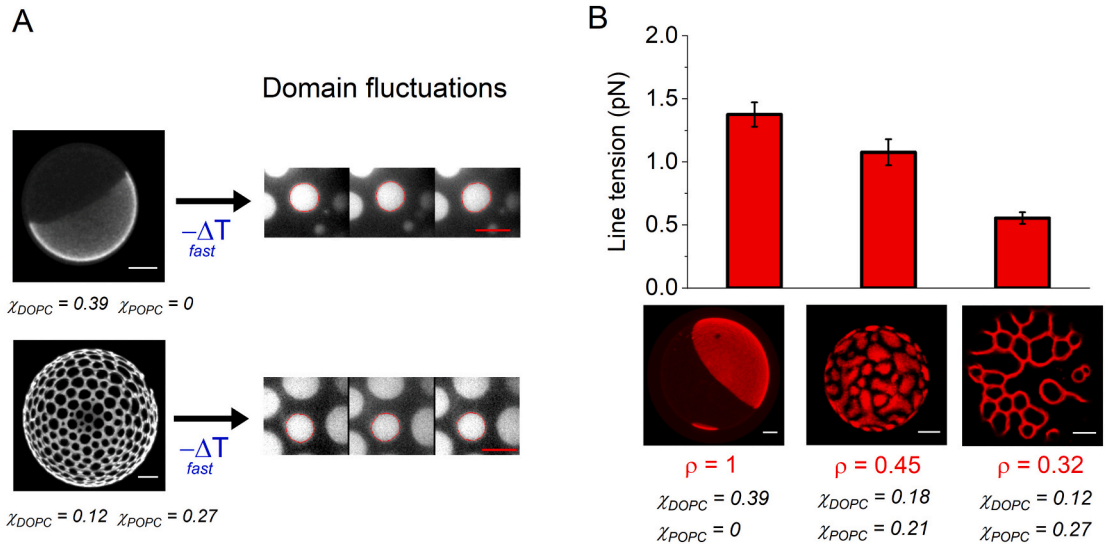

Fig. 2. Phase morphologies and measurements of Ld/Lo line tension. (A) Images used for line tension measurements using flicker spectroscopy. GUVs with macrodomains (upper image) or with modulated phases (lower image) are cooled quickly (−ΔT) in order to facilitate the search for small, round domains ~5 μm diameter. The fluctuations of the edges of these domains are monitored to measure the line tension (see main text and SM). (B) Line tension values obtained from flicker spectroscopy measurements. Bar plots show Ld/Lo line tension for different domain morphologies, indicating a lower line tension when domains form modulated phases. Scale bar 5 μm. Errors are calculated from the standard deviation (n = 8–14 per composition).

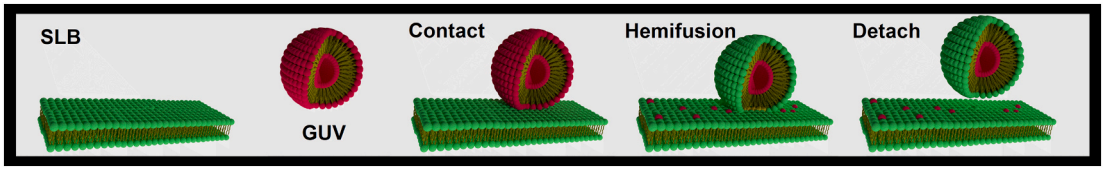

Fig. 3. Hemifusion yields asymmetric GUVs (aGUVs). Diagram shows the experimental procedure. SLB and GUV are prepared with different fluorescent dyes. After the contact of GUV and SLB the addition of the fusogenic agent Ca^{2+} induces hemifusion. The outer leaflet of the GUV and the SLB exchange lipids and dyes. Ions of Ca^{2+} are chelated, and the new aGUV is detached from the SLB.

diffuse through them, enabling the exchange of lipids between the GUV and the SLB. The SLB is a reservoir of new lipids to replace the outer leaflet of the few GUVs that establish contact with the SLB, leading to efficient outer leaflet exchange.

The complete fusion of both bilayers involves the expansion of the hemifusion diaphragm and the formation of a fusion pore [34–38] that creates contact of inner/outer leaflets of GUV and SLB. Indeed, fully-fused GUVs are strongly attached to the SLB, and they are gradually absorbed by the SLB [7]. Conversely, hemifused GUVs are not strongly attached to the SLB, since the contact area between GUVs and SLB is still very small. We monitored the hemifused GUVs in order to avoid the expansion of the hemifusion diaphragm, and interrupted the hemifusion procedure by adding EDTA to chelate Ca^{2+} ions 15–30 min after Ca^{2+} addition. Then we detached the aGUVs form the SLB with a gentle shear force by flushing buffer through the SLB chamber, and pipetting the aGUVs off the SLB (for more details, see Materials and methods).

We previously reported that with the hemifusion method, a small contamination of guest lipids from the SLB are found in the inner leaflet of a small fraction of the hosting aGUVs [7]. We used sodium dithionite to quench the fluorescence of DiD and NBD-PE. DiD was found in both

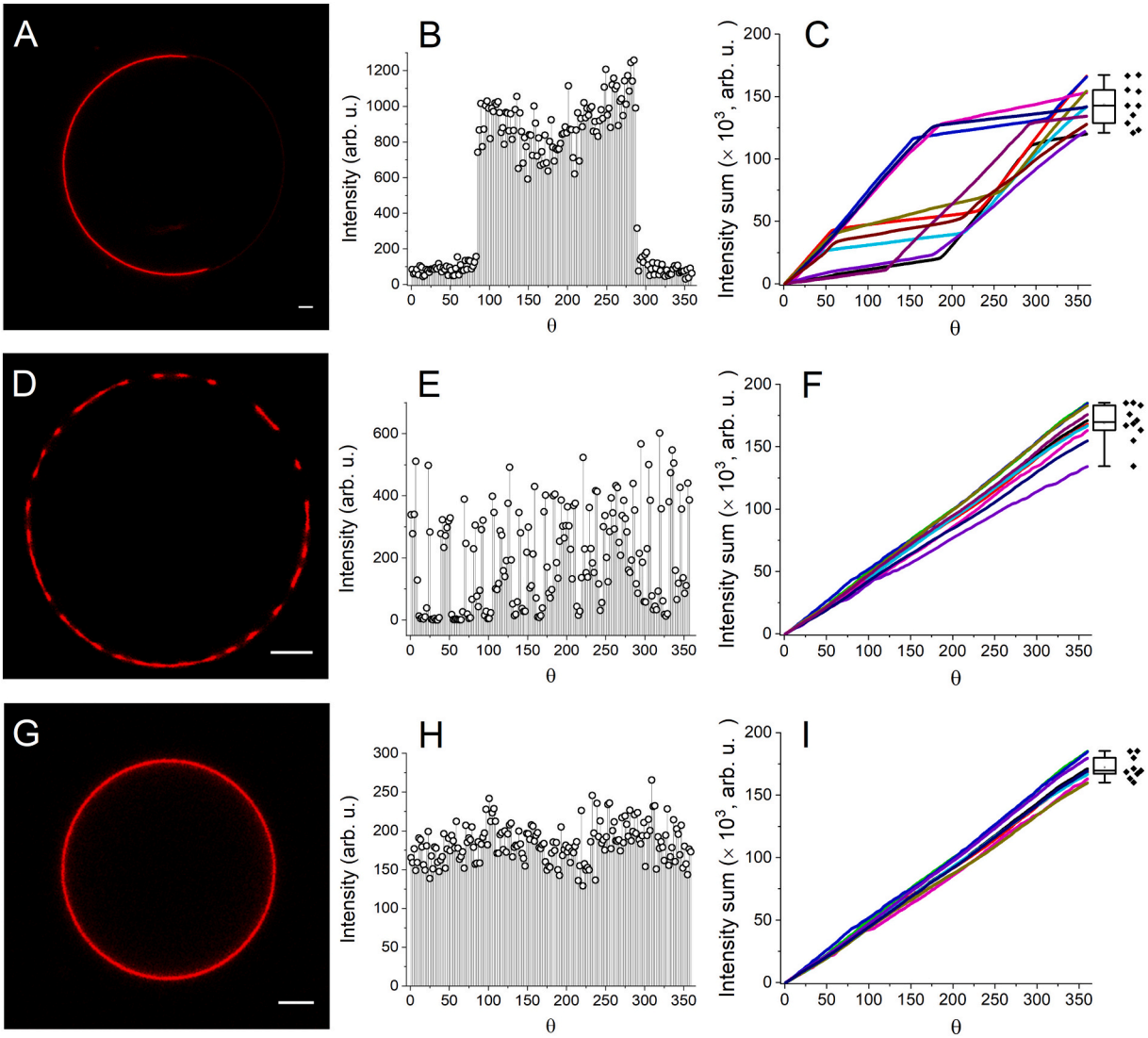

Fig. 4. GUV fluorescence intensity analysis of different Ld + Lo morphologies. The first column shows examples of symmetric control GUV images for different domain morphologies: macrodomains (A); modulated phases (D); and uniform appearance (G). Plots B, E and H (second column) show intensity profiles as a function of the polar angle θ for the vesicles shown in the first column. Plots C, F and I show the corresponding cumulative intensity as a function of θ for several symmetric control GUVs (individual lines), with the box plot representing the distribution (n = 9–10).

leaflets due to the incomplete exchange of the outer leaflet. On the other hand, NBD-PE was found almost exclusively in the outer leaflet. The use of sodium dithionite to quench both dyes resulted in 50% of DiD fluorescence signal, suggesting that the outer leaflet was completed quenched, and the fluorescence of NBD-PE was mostly quenched. We found a small percentage of guest lipids in the inner leaflet of aGUVs, which varies from 5 to 8% of total lipids, and this small percentage was found in ~25% of the aGUVs analyzed [7], similar to results previously observed in asymmetric large unilamellar vesicles [12].

In addition, for the study of asymmetric bilayers, it is important to pay attention to the time stability of the asymmetric state. Note that the hemifusion procedure can be performed in a few minutes 15–30 min, and the observation of aGUVs is completed in a few hours. Since most evidence supports that phospholipids, as used in this work, undergo transbilayer diffusion on a timescale of days to weeks [12,39,40], our observations are hardly affected by phospholipid flip-flop. On the other hand, chol undergoes rapid flip-flop, likely on the timescale of milliseconds to seconds [41–43]. Here, we match the fraction of chol in the GUVs and the SLB, but because of rapid translocation of chol between leaflets, its chemical potential could be essentially identical in both leaflets. Our intuition is that chol is enriched in the inner leaflet of the aGUVs due to preferential interactions with DSPC, but this is not the only contributor to chol chemical potential. It has been suggested that differential stress between leaflets [44] and bending energy [45] are also factors that can influence the transbilayer chol distribution.

3.3. Percentage of lipid exchange of aGUVs

To measure the percentage of lipid that was exchanged between the GUV and the supported bilayer, we compared the intensities of dyes in aGUVs (guest dyes: originally on the SLB, and host dye: originally on the GUV) to the dye intensities in symmetric control GUVs that were not subjected to hemifusion (see Materials and methods). First, we measured the fluorescent dye intensities of control GUVs, and rejected cases of multilamellar vesicles. Fig. 4 shows micrographs of GUVs that exhibit different domain morphologies (Fig. 4A, D and G) and the respective intensity profile as a function of the polar angle, θ (Fig. 4B, E and H).

For phase-separated GUVs with macrodomains (Fig. 4A), intensity vs. θ shows a step-shaped profile (Fig. 4B) in which intensities originating from the Ld and Lo phases are clearly distinct. However, for GUVs with modulated phases (Fig. 4D), intensity vs. θ exhibits multiple intermediate levels (Fig. 4E). Most of the intensities fall between the characteristic values for the pure Ld and Lo phases, making it difficult to assign individual θ values to a particular phase. Instead, we integrated the intensities over θ and plotted the accumulated sum vs. θ. Fig. 4C, F and I shows the cumulative sum of intensity vs. θ of DiD (host dye) measured for different symmetric GUVs (shown as individual lines) for the respective morphologies represented by Fig. 4A, D and G. The intensity value at θ = 360° represents the total sum for a particular GUV, while the box plot represents the distribution of the total intensities for the set of control GUVs.

The cumulative intensity plots for GUVs exhibiting macrodomains (Fig. 4C) are qualitatively different than that from GUVs exhibiting modulated phases (Fig. 4F) or having a uniform appearance (Fig. 4I). In the macrodomain case, accumulated intensity vs. θ for individual GUVs displays regimes with shallower or steeper slopes corresponding to regions of Lo and Ld phases, respectively. In subsequent analyses (for example, Fig. 5) we carefully analyzed these intensities, and only compared GUVs and aGUVs with similar phase fractions (as judged by counting the number of intensities from Ld or Lo divided by their sum) and similar morphologies (i.e., GUVs with macrodomains are compared to aGUVs with macrodomains).

Fig. 5 compares the accumulated intensity vs. θ in asymmetric GUVs (solid lines) with control GUVs labeled with a single dye (lines with symbols). In his kind of plot, we can compare the total intensity of different aGUVs to the total intensities measured in the symmetric GUVs. (For GUVs with uniform appearance, modulated phases or macrodomains, one curve is used as an example.) Interestingly, the comparison of panel (A) and (B) shows that DiD fluorescence decreases and TFPC increases, as the percentage of exchange increases. This observation represents the DiD dye leaving as the TFPC dye enters the aGUV outer leaflet.

The three control GUVs represent the three different observed morphologies: macrodomains (half-filled squares), modulated phases (filled triangles), and nanodomains (open circles). Fig. 5A shows the fluorescence intensity of DiD (the dye originally labeling the symmetric GUV before hemifusion), and Fig. 5B shows the intensity of TFPC (the dye originally in the SLB). After hemifusion and the detachment of the aGUVs from the SLB, aGUVs (solid lines) display a fluorescence signal from both dyes. With increasing extent of lipid exchange in the aGUV, DiD intensity (Fig. 5A) decreases linearly, from its maximum value in the control GUV to half that value. In contrast, TFPC intensity (Fig. 5B) increases linearly, from an initial value of zero to half the value in the symmetric control GUV. The percentage of lipid exchange P for TFPC is

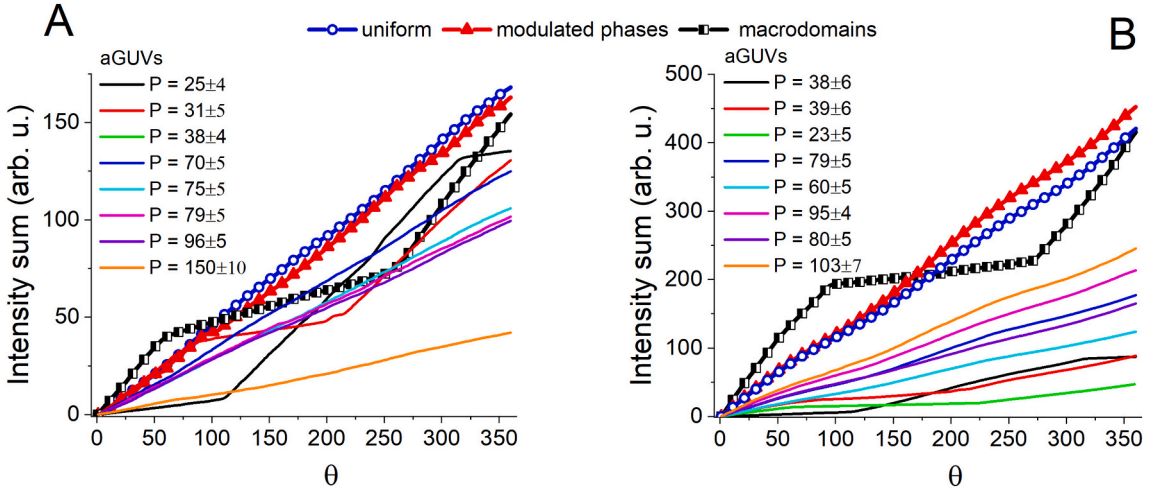

Fig. 5. Comparison of dye fluorescence measured in symmetric control GUVs and aGUVs by use of angular integration around the vesicle equator. (A, B) Intensity sum ($\times 10^3$) as a function of θ for DiD (panel A) and TFPC (panel B) in symmetric GUVs (lines with symbols) and aGUVs (lines only). For aGUVs, the data plotted in A and B correspond to the same aGUV. The total intensity at θ = 360° is used to calculate the percentage of lipid exchange, P. Errors were calculated by propagating the uncertainty using Eq. (3) and considering the standard deviation in the intensities measured in symmetric and aGUVs.

calculated as

$$P = \frac{I_{aGUV}}{I_{GUV}/2} \times 100\% \quad (3)$$

A value of 100% calculated using Eq. (3) indicates complete exchange of the outer leaflet, while a value of 200% would indicate full fusion and complete exchange of both leaflets.

Fig. 5A–B also reveals differences between the percentage of exchange calculated independently from DiD and TFPC intensity. For example, considering the aGUV represented by the black line, analyses of DiD and TFPC indicated 25% and 38% exchange, respectively. Very large differences can be an indication that a vesicle has multiple bilayers. We also occasionally observed >100% exchange (e.g., the orange line in Fig. 5A–B), an indication that some lipids in the inner leaflet were also exchanged. We excluded from our analyses aGUVs showing greater than 100% exchange, or those where DiD and TFPC disagreed by more than 50%.

For a few aGUVs we performed an additional control experiment of tracking individual aGUVs during heating, monitoring temperature in the sample chamber using a thermocouple. Upon heating to 50 °C, aGUV became uniform in appearance, indicating a single Ld phase. We compared the fluorescence intensity of these aGUVs to the intensities of control GUVs at the same temperature of 50 °C. Analysis of uniform GUVs/aGUVs allowed for a straightforward calculation of the percentage of lipid that was exchanged during hemifusion. The purple line in Fig. 5 shows an example of an aGUV with modulated phases that was subjected to this test. Analysis of images collected at 23 °C showed 96% and 80% exchange using DiD and TFPC intensity, respectively. For images of the same aGUV collected at 50 °C, exchange was 98% and 84% for DiD and TFPC, respectively. This additional control experiment was performed in order to validate the analyses that use the intensity sum to calculate the percentage of lipid exchange.

Fig. 6 shows correlation plots of the exchange values calculated independently for the two fluorescent probes, DiD and TFPC. In such a plot, a line with slope = 1 represents perfect agreement between these two dyes. Independent experiments were performed starting with symmetric GUVs of different ρ values, which were subsequently hemifused with an SLB composed of DOPC/chol = 0.8/0.2. After hemifusion, aGUVs have an inner leaflet with the lipid composition of the initial symmetric GUV, and an outer leaflet with increased fractions of DOPC. The fraction of chol was chosen to be the same for the initially symmetric GUVs and the SLB, leading (at least initially) to the same fraction of chol in both leaflets of the aGUVs.

Fig. 6A shows the percentage of lipid exchange obtained for aGUVs with inner leaflet composition at ρ = 0.32, where symmetric GUVs with this lipid composition exhibit approximately 80% of GUVs with modulated phases and 20% of GUVs with macrodomains (see Fig. 1C). After hemifusion, aGUVs with a low percentage of exchange < 40% exhibited the domain morphologies observed in the original symmetric GUVs, either modulated phases or macrodomains. For aGUVs with a greater percentage of exchange, modulated phases or macrodomains were no longer observed; instead, the vesicles appeared uniform. As we explain in detail below, the percentage of exchange is a key parameter for interpreting the influence of one leaflet on another. Here, we grouped as highly asymmetric vesicles those aGUVs with a percentage of lipid exchange > 60%. For this group of aGUVs, the bilayer asymmetry causes a dramatic change in the domain morphology, with vesicles now showing a uniform appearance in micrographs. These results imply in a large shift in the ρ-window of these aGUVs compared to the initially symmetric GUVs, as discussed below. Fig. 6B shows results obtained for aGUVs with different lipid composition in the inner leaflet (ρ values indicated in the legend). The solid colored lines in Fig. 6B represent the lines of slope 1 for each composition, and the symbols in this plot represent different morphologies as given by Fig. 6A legend.

3.4. Increasing asymmetry changes bilayer phase behavior

The percentage of lipid exchange plays an important role in the interpretation of asymmetric bilayers. Previously, we showed that the physical-chemical properties of aGUVs change as the percentage of asymmetry increases [7]. Fig. 7A and B shows examples of two different symmetric GUVs with ρ = 0.45 labeled exclusively with TFPC or DiD, respectively.

Fig. 7C shows the phase diagram and the lipid composition of the symmetric GUVs (star) displayed in Fig. 7A and B. The line that connects the ternary phase diagrams DSPC/DOPC/chol (near face of the tetrahedron) and DSPC/POPC/chol (far face of the tetrahedron) represents the trajectory of lipid compositions studied in this work. Moreover, Ld and Lo phase boundaries are represented by the lines colored red and blue, respectively, with the critical point found in between these lines. Phases boundaries and critical points were obtained in a previous report [31].

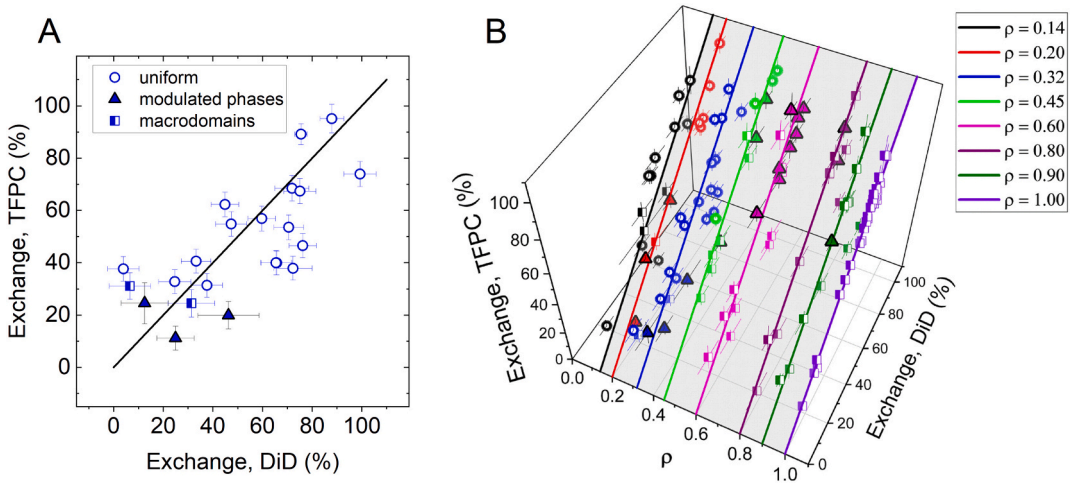

Fig. 6. Percentage of lipid exchange in aGUVs measured by two different dyes. (A) An example of the percentage of lipid exchange calculated for DiD and TFPC in the aGUVs. The line of slope 1 represents 100% agreement between the percentages of exchange reported by both dyes. The symbols represent different domain morphologies: uniform (open circle), modulated phases (filed triangles) and macrodomains (half-filled squares). For aGUVs shown in (A) the inner leaflet has the composition described as ρ = 0.32, and high percentage of exchange reflects increasing fractions of DOPC on the outer leaflet. (B) Percentage of lipid exchange calculated for both DiD and TFPC in aGUVs with different inner leaflet compositions. The inner leaflet composition is equivalent to the lipid composition of symmetric GUVs before hemifusion.

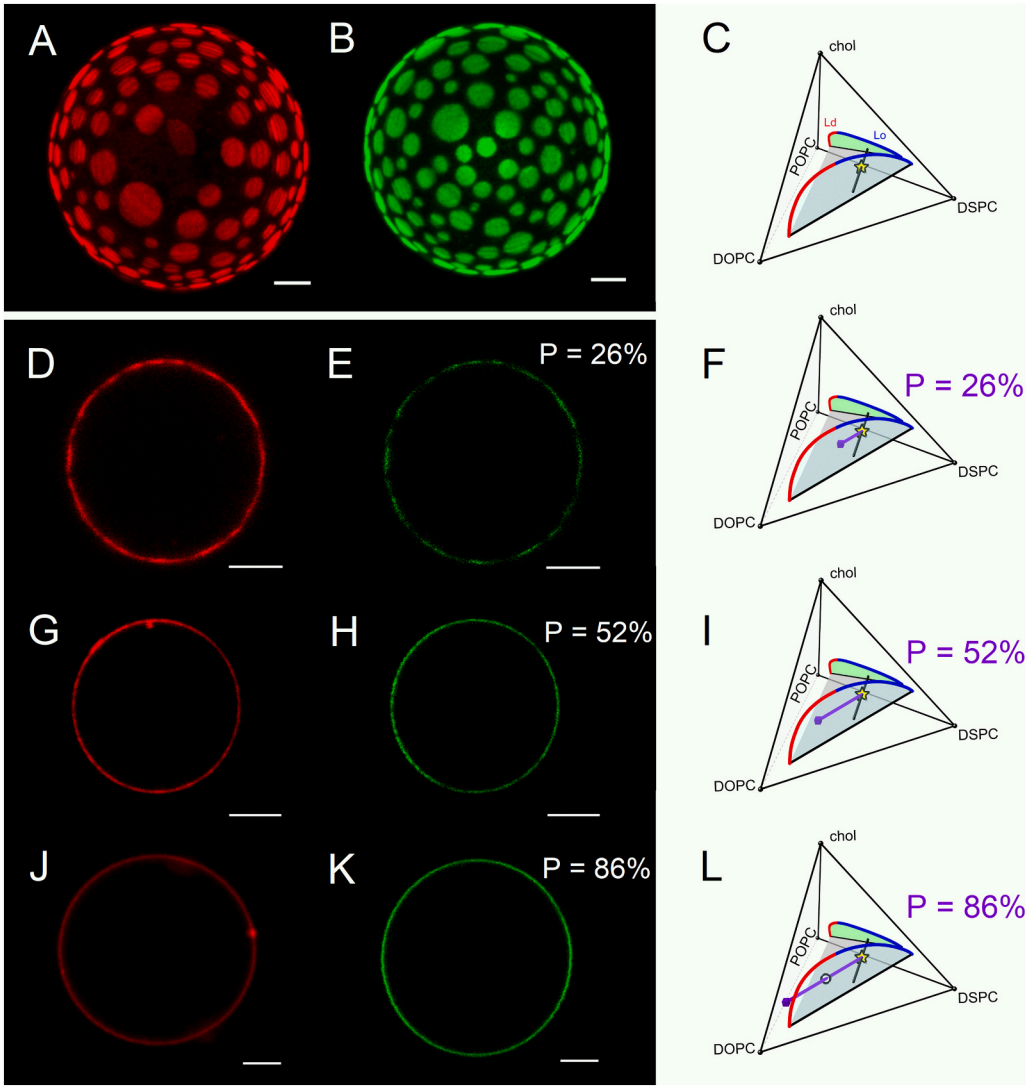

Fig. 7. High percentage of lipid exchange removes remnants of phase separation, ensuring a fluid outer leaflet. (A, B) Images of symmetric different GUVs labeled with DiD and TFPC, respectively. (C) Tetrahedron shows the phase diagram of DSPC/DOPC/POPC/chol, where the ternary phase diagrams of DSPC/DOPC/chol and DSPC/POPC/chol are highlighted in the near and far faces of the tetrahedron. The phase boundaries displayed in red and blue represent the Ld and Lo phases boundaries that separate the one- from the two-phase region. The star represents the lipid composition of symmetric GUVs (C, F, I, L), and the line crossing the tetrahedron and through this point represents the ρ-trajectory studied in this work. The following sequence of images displays aGUVs with different percentage of exchange. The first column (images D, G and J) and second column (images E, H and K) are the fluorescence of DiD and TFPC, respectively, from the same aGUV. Here, DiD and TFPC signal reports registered leaflets. The third column (tetrahedrons F, I and L) shows the lipid composition of the inner leaflet (star) and the lipid composition of the outer leaflet (purple square connected to the star). The extension of the line that connects the inner and outer leaflet compositions is related to the percentage of lipid exchange, P. In L the open circle displays the lipid composition that would be expected for scrambled bilayers.

The sequence of images in Fig. 7D, E, G, H, J, and K shows aGUVs after hemifusion and lipid exchange, with the aGUVs now containing both DiD and TFPC. Each row displayed in the sequence of images in Fig. 7D–E, G–H and J–K now represents the same aGUV that is visualized in red and green channels in the microscope. For these rows (D–E, G–H and J–K), images represent increasing percentages of lipid exchange between the GUV and the SLB, with the aGUV in J-K having highest percentage of asymmetry, 86%. Symmetric GUVs shown in Fig. 7A–B have the lipid composition DSPC/DOPC/POPC/chol = 0.39/0.18/0.21/0.22, and display macro and broken Ld domains surrounded by a continuous Lo phase. These symmetric GUVs show distinct Ld and Lo phases, where the intensity in the Ld domains is approximately 7–10 times brighter than the intensity in the Lo domains. GUVs with this composition, labeled exclusively with DiD (red fluorescence), are hemifused to a SLB composed of DOPC/chol = 0.8/0.2.

After hemifusion and detachment of the aGUVs from the SLB, we observe a population of aGUVs with different percentages of lipid exchange. Fig. 7D–E shows an example where 26% of the outer leaflet was exchanged with DOPC/chol (0.8/0.2). We calculate the lipid composition in the outer leaflet for this aGUV (Fig. 7D, E) to be 0.74 × (DSPC/DOPC/POPC/chol = 0.39/0.18/0.21/0.22) + 0.26 × (DSPC/DOPC/POPC/chol = 0/0.8/0/0.2) = DSPC/DOPC/POPC/chol = 0.29/0.34/0.16/0.21, whereas the lipid composition of the inner leaflet remains equal to that of the previous symmetric GUV before hemifusion. Fig. 7F shows these lipid compositions on the phase diagram, where the star and the square represent the inner and the outer leaflet lipid composition, respectively. With 26% outer leaflet exchange, the inner and the outer leaflets have a lipid composition that forms Ld and Lo domains, although the outer leaflet is slightly enriched in DOPC (see purple square). Therefore, Fig. 7D–E shows that this aGUV still forms Ld/Lo domains in each leaflet. The red and the green channel also shows the alignment of domains between the inner and the outer leaflet, although the domains are less distinct than in the images of symmetric GUVs (Fig. 7A–B). Compared to symmetric GUVs, the dye partition coefficient between Ld and Lo phases of the fluorescent probes DiD and TFPC decreased for aGUVs [7], and the domains also became slightly smaller. Fig. 7G–H shows an aGUV with 52% outer leaflet exchange. The lipid composition of the inner and outer leaflets are DSPC/DOPC/POPC/chol = 0.39/0.18/0.21/0.22 and DSPC/DOPC/POPC/chol = 0.19/0.50/0.10/0.21, respectively (Fig. 7I). Although the aGUV appears to be more uniform, there are still a few detectable dark Lo domains. In addition, the red and the green channel each report similar behavior, indicating coupled leaflets.

We observe a qualitatively different behavior for an aGUV with 86% outer leaflet exchange, shown in Fig. 7J–K. For the vesicle, which has an outer leaflet lipid composition DSPC/DOPC/POPC/chol = 0.06/0.71/0.03/0.20, the aGUVs appear uniform. As shown in Fig. 7L, the outer leaflet composition is now outside the two-phase region of the phase

diagram for symmetric GUVs. Although the phase diagram for symmetric and asymmetric bilayers may be different [5], for 86% lipid exchange, the outer leaflet of this aGUV seems to form a uniform fluid phase. Interestingly, for this aGUV having a high percentage of asymmetry in which the outer leaflet is estimated to be a uniform Ld phase, we observe a change in the domain morphology compared to the symmetric GUVs in Fig. 7A–B, in which GUVs display macrodomains and aGUVs have a uniform appearance. For all percentages of lipid exchange discussed, the inner and the outer leaflet exhibit aligned domains. However, we observed that a few percent of aGUVs (5–10%) show anti-alignment of domains between the inner and the outer leaflet (see Data in Brief co-submission). Here, we have not investigated domain anti-registration.

The total lipid composition of the aGUV displayed in Fig. 7J–K is estimated as the composition of the inner leaflet DSPC/DOPC/POPC/chol = (0.39/0.18/0.21/0.22 + the composition of the outer leaflet DSPC/DOPC/POPC/chol = 0.06/0.71/0.03/0.20) / 2, which is equivalent to DSPC/DOPC/POPC/chol = 0.22/0.45/0.12/0.21 (open circle in the two-phase region of the tetrahedron, Fig. 7L). For 86% lipid exchange of one leaflet, if the inner and outer leaflets were to equilibrate their lipid compositions, the GUV with such composition would phase-separate into Ld + Lo domains. In other words, if the lipids from the aGUVs shown in Fig. 7J–K were scrambled to create a symmetric GUV, that symmetric vesicle would be phase-separated instead of showing a uniform appearance. This simple explanation also corroborates the evidence that the studied aGUV is asymmetric.

3.5. Line tension is reduced in asymmetric GUVs

Since the percentage of lipid exchange strongly influences the phase properties of the bilayer, we focused the next part of our study on only highly asymmetric aGUVs having a large percentage of lipid exchange. We compared the domain morphologies of aGUVs with >60% lipid exchange to the morphologies observed in symmetric GUVs. Fig. 8A shows a sequence of images for symmetric GUVs labeled with DiD (top row, red fluorescence), and asymmetric GUVs labeled with TFPC (bottom row, green fluorescence), for different values of ρ. We note that although TFPC that labels only the outer leaflet of the aGUVs, both the inner and outer leaflets show the same domain morphology, meaning that the leaflets are registered. Although the outer leaflet lipid compositions of the aGUVs in Fig. 8A were slightly different, given the high percentage of exchange, they were mostly composed of DOPC (>60%) and 20% chol. These numbers were obtained by the calculations of lipid exchange for the aGUVs shown in Fig. 7. More importantly, such compositions should form a uniform fluid phase according to the phase diagram of symmetrical bilayers, and the discussion above, Fig. 7. Interestingly, compared to the symmetric bilayer that exhibits modulated phases (ρ = 0.32, second column in Fig. 8A), the new outer leaflet enriched in DOPC erased the Ld and Lo patterns on the bilayer, and the aGUV had a uniform appearance. In addition, the macrodomains formed

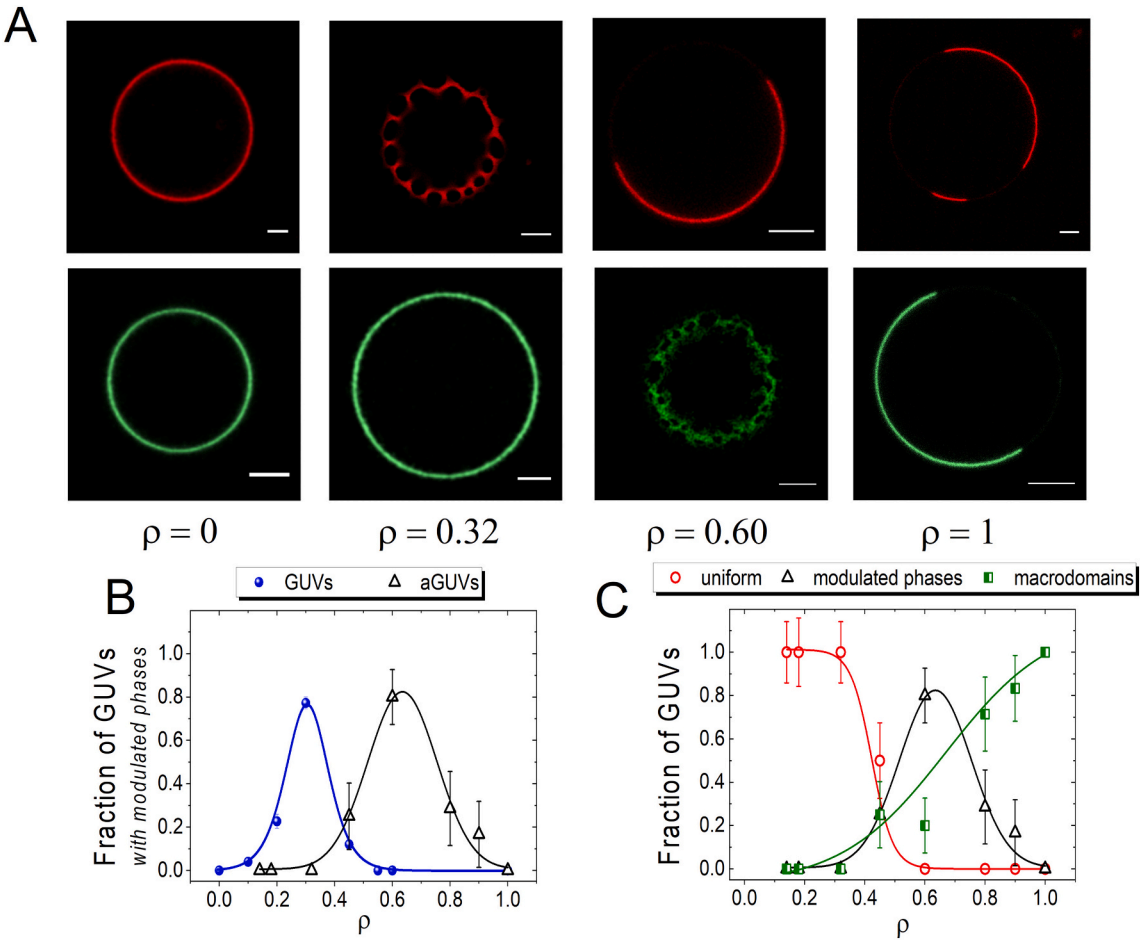

Fig. 8. Comparison of modulated phases in symmetric and asymmetric GUVs. (A) Micrographs of symmetric GUVs (upper images) and aGUVs (lower images). From left to right, the sequence of images represents ρ = 0, ρ = 0.32, ρ = 0.6 and ρ = 1. For aGUVs, the nomenclature ρ refers to the inner leaflet. (B) the window in lipid composition where the majority of the GUVs and aGUVs (with percentage of exchange > 60%) exhibit modulated phases. For aGUVs this window is shifted to higher values of ρ, indicating a decrease of the Ld/Lo line tension. Here, all aGUVs examined have percentages of exchange greater than 60%. (C) the fraction of aGUVs with modulated phases, uniform appearance or macrodomains. Errors are calculated from the standard deviation (n = 9–22 per composition).

in the symmetric case for ρ = 0.6 (third column in Fig. 8A) changed to modulated phases once the outer leaflet of the aGUV was replaced by a composition of a single Ld phase. These observations are consistent with the increase of Ld + Lo contact perimeter, indicating a decrease of Ld/Lo line tension. Although the outer leaflet has the lipid composition of a fluid phase, the inner and the outer leaflet form modulated phases. For ρ = 1, aGUVs exhibited macroscopic domains. These vesicles have an outer leaflet composition DOPC/chol ≅ 0.8/0.2, but clearly show domains in the outer leaflet that were induced by the inner leaflet. Indeed, we previously reported these domains to have different properties compared to the symmetric Ld and Lo phases [7] (see discussion below).

Fig. 8B and C shows the counted frequency that these changes in the domain morphologies occur. Fig. 8B shows the fraction of GUVs or aGUVs with modulated phases. Comparing symmetric and asymmetric bilayers, for aGUVs, we observe that modulated phases occurred at higher values of ρ (i.e., a higher fraction of DOPC and lower fraction of POPC). As described in Figs. 1 and 2, increasing fractions of POPC lead to a decrease of Ld/Lo domain line tension in symmetric vesicles. Fig. 8B shows that the fraction of POPC needed to form modulated phases is smaller in aGUVs than in symmetric GUVs, implying that aGUVs have asymmetric domains with an intrinsically lower line tension. Fig. 8C shows the fraction of aGUVs that appear uniform, or with modulated phases, or with macrodomains. For example, for ρ = 0.32, ≈80% of symmetric GUVs display modulated phases (Fig. 8B) whereas almost 100% of aGUVs are found to be uniform (Fig. 8C). Moreover, for ρ = 0.6, almost all symmetric GUVs exhibit macrodomains (see Fig. 1C), whereas about 80% of aGUVs exhibit modulated phases + 20% macrodomains. As mentioned above, the ρ-window marks the domain size transition from nano- to macrodomains [16]. The shift of the ρ-window to higher values of ρ is known to stabilize the regime of nanometer-sized domains. We plan a future investigation of nanometer-sized domains in aGUVs. Although we have not verified that any of the compositions that precede the ρ-window form nanodomains, our results are consistent with decreased line tension in aGUVs.

Measuring the Ld/Lo line tension directly, for example, by use of flicker spectroscopy as we have done for symmetric GUVs, is not feasible for aGUVs. Instead, we compared where modulated phases appear in symmetric and aGUVs. Based on our previous study of line tension in symmetric GUVs where we could directly measure line tension, appearance of modulated phases corresponds to a lowering of line tension in these mixtures from ~1.4 pN (macrodomains) down to between 0.3 and 0.6 pN, the line tension ranges for modulated phases. In a symmetric GUV with both leaflets phase-separated, a simple model of the measured line tension involves the sum of line tensions from each leaflet [46]. In aGUVs, if we disregard the coupling between the leaflets, the observed decrease of line tension is in the ballpark of what we would predict from complete loss of the in-register interfacial energy from one leaflet. This simple model does not account for the interaction at the middle of the bilayer where the phase-separated domains are in contact with the initially uniform leaflet, but agree with our experimental observation.

3.6. Inter- and intra-leaflet interactions

In our previous work, we studied aGUVs in which the inner leaflet phase separates into macrodomains, whereas the outer leaflet is DOPC/chol (0.8/0.2) [7]. Although these aGUVs presumably have lipid compositions forming different domain morphologies (with domains on the inner leaflet, and one single uniform phase on the outer leaflet), the fluorescent dyes that report the phase behavior of each individual leaflet show that both leaflets phase-separate into macrodomains (as we observed here, see Fig. 8A, ρ = 1). This observation suggests that the phase-separated leaflet induces domains in the opposed fluid phase of the outer leaflet. However, asymmetric domains on aGUVs have a significantly lower dye partition coefficient compared to symmetric Ld and Lo phases on GUVs. The observed lower dye partition coefficient suggests that the Ld and the Lo phases are more alike in terms of lipid packing/order, and possibly in terms of lipid composition [7]. For the outer leaflet mainly composed of DOPC/chol (0.8/0.2), the induced domains might involve chol preferentially locating across from the inner Lo phase [7,47]. Indeed, the partition coefficient of TFPC in the outer leaflet was measured to be $Kp^{TFPC,\ aGUV} = 3.6 \pm 1.4$ suggesting a slight difference in lipid composition and lipid order between the induced ordered and disordered domains in this leaflet [7]. In a previous study, we used the fluorescent probe C-Laurdan to measure the lipid packing/order of the asymmetric domains. We found that the difference in lipid packing/order between the asymmetric ordered and disordered domains is ~25% smaller than the order difference observed between the symmetric Ld and Lo phases [7]. Therefore, the asymmetric ordered and disordered domains are indeed more alike in terms of lipid packing/order. In part, the fluid and disordered outer leaflet influences the lipid packing of the phase-separated inner leaflet. A similar effect was observed in asymmetric LUVs using small-angle neutron scattering, where it was found that a highly fluid leaflet reduced the packing density of ordered domains in the opposing leaflet [12]. Moreover, this Ld outer leaflet could induce a slight re-distribution of lipids and chol between the inner Ld and Lo phases [7]. The re-distribution of high Tm lipid, low Tm lipid and chol in the phase-separated inner leaflet contributes to the decrease of the difference in order between ordered and disordered asymmetric domains. In addition, we also observed that the asymmetric ordered domain is significantly less ordered than the symmetric Lo phase.

A highly packed/ordered phase across from a disordered phase must involve some unfavorable contact energy in the bilayer midplane. In these asymmetric bilayers, the disorder of the fluid outer leaflet affects the phase-separated inner leaflet, mostly affecting the order of the Lo phase, in addition to possibly a slight redistribution of lipids that contributes to decreased order of the inner Lo phase [7]. In the presence of a lipid such as POPC (i.e., a lower ρ-value), the line tension decreases. Thus, the mechanism discussed above of the fluid leaflet possibly inducing a reorganization of the lipid in the phase-separated leaflet, can contribute to breaking the domains into even smaller domains. It should be noted that the domain morphology is only affected when the line tension decreases to a certain level, i.e. at high line tension such as ρ = 1 the influence of the fluid leaflet is not enough to break the domains apart, but it does so for ρ = 0.6 (Fig. 8). Thus, in this study we can identify two main fundamental interactions that drive the lipid phase behavior. The intra-leaflet (intra-plane) interaction is related to the line tension, or the unfavorable interaction of two distinct phases in lateral contact. The inter-leaflet (inter-plane) interaction is related to how both leaflets affect each other, possibly changing the lipid packing/order across the bilayer, “transmembrane lipid packing”. Thus, the inter-plane interaction is also related to the leaflet coupling. The competition between these interactions explains our observations. For a high line tension, for instance as observed at ρ = 1, the presence of a fluid leaflet opposed to a phase-separated leaflet affects the properties of the bilayer, as the lipid packing/order [7], but not strongly enough to change the domain morphology. On the other hand, for ρ = 0.6 compared to ρ = 1, the line tension is slightly smaller due to the presence of POPC, and now the influence of a fluid outer leaflet opposed to the phase-separated leaflet changes the domain morphology, giving rise to modulated phases (see Fig. 8). As discussed above in Fig. 2, the observed change in the domain morphology from macrodomains to modulated phases leads to a decrease in the Ld/Lo line tension by a factor of 2–3, Fig. 2B.

Line tension is commonly discussed in the literature in terms of the hydrophobic mismatch between thickness of Ld and Lo phases [48]. Here, we emphasize the line tension as an interaction between two phases in contact and not only due to the hydrophobic mismatch [46]. There is experimental evidence that hydrophobic mismatch and line tension can be correlated but this has not been shown to be a causal connection. Heberle et al. [23] reported that the Ld/Lo thickness mismatch decreases with the increase of the fraction of POPC (decrease

of ρ), as shown in Fig. 2 the line tension follows the same trend. Thus, the decrease of Ld/Lo thickness mismatch is associated with the decrease of the Ld/Lo line tension [16]. Looking at the hydrophobic mismatch of asymmetric membranes, Wang and London [14] investigated asymmetric bilayers, in which one leaflet is phase-separated, and another is enriched in the fluid lipid DOPC. In their experiments, they compared the melting transition of Ld + Lo domains for a series of ternary mixtures in the phase-separated leaflet; the high Tm lipids studied in their work have different chain lengths. Interestingly, for the series of PC headgroups, Wang and London found that for the mixture with highest hydrophobic mismatch, i.e. highest line tension, there is a higher tendency to maintain the domain phase separation in asymmetric vesicles [14]. For the mixture of the lowest thickness mismatch, and therefore for a line tension that has decreased to a certain level, they observed that the initially phase-separated leaflet becomes uniform due to the influence of the fluid, DOPC-enriched leaflet [14]. The results of Wang and London [14] can also be explained by the competing inter- and intra-plane interactions that here we first contrapose with the experimental evidence.

A number of theoretical studies have investigated interleaflet coupling in asymmetric lipid bilayers [4,5,48]. Collins [49] proposed that the key interaction is a surface tension between the two leaflets. Different from the line tension energy that scales with domain perimeter, it is suggested that this interfacial energy scales with the area and favors liquids on either side of the midplane to be identical [49]. May [4] estimated the mismatch energy, which is the energy penalty for having an Ld phase across from an Lo phase compared to the symmetric case. May concluded that dynamic chain interdigitation is likely the largest contributor to the interleaflet coupling constant, whereas electrostatic interactions and cholesterol flip-flop are approximately an order of magnitude smaller [4]. Putzel et al. [50] found that gauche bond energy, orientational interactions, and chain configurational entropy contribute to the mismatch energy. They suggested that since these contributions are constrained in a complex way, the interleaflet coupling cannot be traced to a single factor [50]. Estimates of the mismatch energy span nearly two orders of magnitude, ranging from ~0.5 k_BT/nm^2 [49], ~0.1–0.2 k_BT/nm^2 [51] and 0.01–0.03 k_BT/nm^2 [50].

Here, we do not have any method to estimate an interleaflet coupling energy, but instead measure the more readily interpreted influence on line tension in the phase-separated leaflet. Therefore, we prefer not to speculate on the molecular nature of the leaflet coupling, which we feel requires its own systematic investigation. Instead, we focus on how a leaflet having a mixture composition that would yield a single phase were it a symmetrical bilayer, can influence the Ld/Lo line tension, and hence phase domain size, of a coupled phase-separated leaflet.

4. Conclusions

We investigated the line tension of asymmetric domains. Line tension is the key parameter that affects the domain size. Therefore, the existence of domains in model membranes, or “lipid rafts” in the cell, is correlated to this fundamental interaction that originates from the domain interface where Ld and Lo phases are in contact. We showed that the domain line tension could be systematically studied by monitoring the phase morphology of coexisting Ld and Lo domains. Thus, compared to macroscopic phase separation, the appearance of modulated phases is associated with an increase in the contact perimeter of Ld/Lo phases, indicating a decrease of the domain line tension. We prepared aGUVs via hemifusion, where the inner leaflet is phase separated and the outer leaflet forms induced asymmetric domains when consisting mostly of DOPC/chol = 0.8/0.2, a genuinely fluid lipid composition. This method enables selection and study of aGUVs exhibiting a high percentage of asymmetry, in which most of the outer leaflet of aGUVs was exchanged with the desired lipid composition. Comparing our results for GUVs and aGUVs, we found that the interaction between a phase-separated and fluid leaflet (DOPC/chol) lowers the line tension of asymmetric domains.

CRediT authorship contribution statement

TAE performed the experiments, analyzed the data, and wrote the first draft of the manuscript; JW performed experiments with symmetric GUVs; FAH and GWF co-wrote the manuscript and performed research; TAE and GWF designed the experiments.

Declaration of competing interest

The authors declare that they have no known competing financial interests or personal relationships that could have appeared to influence the work reported in this paper.

Acknowledgements

We thank David Ackerman for writing the line tension code in GWF’s group. We previously reported line tension measurements using this code. F.A.H. and T.A.E. were supported by NSF Grant MCB-1817929. This work was also supported by National Institutes of Health grant R01GM105684 (G.W.F. and T.A.E.). TAE also thanks the CNPq for support in the beginning of this project.

Appendix A. Supplementary data

Supplementary data to this article can be found online at https://doi.org/10.1016/j.bbamem.2021.183586.

References

[1] I. Levental, S.L. Veatch, The continuing mystery of lipid rafts, J. Mol. Biol. 428 (2016) 4749–4764, https://doi.org/10.1016/j.jmb.2016.08.022.
[2] J.H. Lorent, K.R. Levental, L. Ganesan, G. Rivera-Longsworth, E. Sezgin, M. Doktorova, E. Lyman, I. Levental, Plasma membranes are asymmetric in lipid unsaturation, packing and protein shape, Nat. Chem. Biol. 16 (2020) 644–652, https://doi.org/10.1038/s41589-020-0529-6.
[3] G. van Meer, D.R. Voelker, G.W. Feigenson, Membrane lipids: where they are and how they behave, Nat. Rev. Mol. Cell Biol. 9 (2008) 112–124, https://doi.org/10.1038/nrm2330.
[4] S. May, Trans-monolayer coupling of fluid domains in lipid bilayers, Soft Matter 5 (2009) 3148–3156, https://doi.org/10.1039/b901647c.
[5] A.J. Wagner, S. Loew, S. May, Influence of monolayer-monolayer coupling on the phase behavior of a fluid lipid bilayer, Biophys. J. 93 (2007) 4268–4277, https://doi.org/10.1529/biophysj.107.115675.
[6] H.T. Cheng, E. London Megha, Preparation and properties of asymmetric vesicles that mimic cell membranes. Effect upon lipid raft formation and transmembrane helix orientation, J. Biol. Chem. 284 (2009) 6079–6092, https://doi.org/10.1074/jbc.M806077200.
[7] T.A. Enoki, G.W. Feigenson, Asymmetric bilayers by hemifusion: method and leaflet behaviors, Biophys. J. 117 (2019) 1037–1050, https://doi.org/10.1016/j.bpj.2019.07.054.
[8] P. Pathak, E. London, Measurement of lipid nanodomain (Raft) formation and size in sphingomyelin/POPC/cholesterol vesicles shows TX-100 and transmembrane helices increase domain size by coalescing preexisting nanodomains but do not induce domain formation, Biophys. J. 101 (2011) 2417–2425, https://doi.org/10.1016/j.bpj.2011.08.059.
[9] S. Pautot, B.J. Frisken, D.A. Weitz, Engineering asymmetric vesicles, Proc. Natl. Acad. Sci. U. S. A. 100 (2003) 10718–10721, https://doi.org/10.1073/pnas.1931005100.
[10] M.D. Collins, S.L. Keller, Tuning lipid mixtures to induce or suppress domain formation across leaflets of unsupported asymmetric bilayers, Proc. Natl. Acad. Sci. 105 (2008) 124–128, https://doi.org/10.1073/pnas.0702970105.
[11] S. Chiantia, P. Schwille, A.S. Klymchenko, E. London, Asymmetric GUVs prepared by MβCD-mediated lipid exchange: an FCS study, Biophys. J. 100 (2011) L1–L3, https://doi.org/10.1016/j.bpj.2010.11.051.
[12] F.A. Heberle, D. Marquardt, M. Doktorova, B. Geier, R.F. Standaert, P. Heftberger, B. Kollmitzer, J.D. Nickels, R.A. Dick, G.W. Feigenson, J. Katsaras, E. London, G. Pabst, Subnanometer structure of an asymmetric model membrane: interleaflet coupling influences domain properties, Langmuir 32 (2016) 5195–5200, https://doi.org/10.1021/acs.langmuir.5b04562.
[13] B. Eicher, D. Marquardt, F.A. Heberle, I. Letofsky-Papst, G.N. Rechberger, M.-S. Appavou, J. Katsaras, G. Pabst, Intrinsic curvature-mediated transbilayer coupling in asymmetric lipid vesicles, Biophys. J. 114 (2018) 146–157, https://doi.org/10.1016/j.bpj.2017.11.009.
[14] Q. Wang, E. London, Lipid structure and composition control consequences of interleaflet coupling in asymmetric vesicles, Biophys. J. 115 (2018) 664–678, https://doi.org/10.1016/j.bpj.2018.07.011.

[15] J.W. St. Clair, E. London, Effect of sterol structure on ordered membrane domain (raft) stability in symmetric and asymmetric vesicles, Biochim. Biophys. Acta Biomembr. 1861 (2019) 1112–1122, https://doi.org/10.1016/j.bbamem.2019.03.012.
[16] R.D. Usery, T.A. Enoki, S.P. Wickramasinghe, M.D. Weiner, W.C. Tsai, M.B. Kim, S. Wang, T.L. Torng, D.G. Ackerman, F.A. Heberle, J. Katsaras, G.W. Feigenson, Line tension controls liquid-disordered + liquid-ordered domain size transition in lipid bilayers, Biophys. J. 112 (2017) 1431–1443, https://doi.org/10.1016/j.bpj.2017.02.033.
[17] F.A. Heberle, J.T. Buboltz, D. Stringer, G.W. Feigenson, Fluorescence methods to detect phase boundaries in lipid bilayer mixtures, Biochim. Biophys. Acta Mol. Cell Res. 1746 (2005) 186–192, https://doi.org/10.1016/j.bbamcr.2005.05.008.
[18] R.S. Petruzielo, F.A. Heberle, P. Drazba, J. Katsaras, G.W. Feigenson, Phase behavior and domain size in sphingomyelin-containing lipid bilayers, Biochim. Biophys. Acta 1828 (2013) 1302–1313.
[19] G.W. Feigenson, J.T. Buboltz, Ternary phase diagram of dipalmitoyl-PC/dilauroyl-PC/cholesterol: nanoscopic domain formation driven by cholesterol, Biophys. J. 80 (2001) 2775–2788, https://doi.org/10.1016/S0006-3495(01)76245-5.
[20] G.W. Feigenson, Phase behavior of lipid mixtures, Nat. Chem. Biol. 2 (2006) 560–563, https://doi.org/10.1038/nchembio1106-560.
[21] T.M. Konyakhina, S.L. Goh, J. Amazon, F.A. Heberle, J. Wu, G.W. Feigenson, Control of a nanoscopic-to-macroscopic transition: modulated phases in four-component DSPC/DOPC/POPC/Chol giant unilamellar vesicles, Biophys. J. 101 (2011) L8–L10, https://doi.org/10.1016/j.bpj.2011.06.019.
[22] T.A. Enoki, F.A. Heberle, G.W. Feigenson, FRET detects the size of nanodomains for coexisting liquid-disordered and liquid-ordered phases, Biophys. J. 114 (2018) 1921–1935. https://www.sciencedirect.com/science/article/pii/S0006349518303801.
[23] F.A. Heberle, R.S. Petruzielo, J. Pan, P. Drazba, N. Kučerka, R.F. Standaert, G. W. Feigenson, J. Katsaras, Bilayer thickness mismatch controls domain size in model membranes, J. Am. Chem. Soc. 135 (2013) 6853–6859, https://doi.org/10.1021/ja3113615.
[24] F.A. Heberle, M. Doktorova, H.L. Scott, A.D. Skinkle, M.N. Waxham, I. Levental, Direct label-free imaging of nanodomains in biomimetic and biological membranes by cryogenic electron microscopy, Proc. Natl. Acad. Sci. U. S. A. 117 (2020) 19943–19952, https://doi.org/10.1073/PNAS.2002200117.
[25] C. Eggeling, C. Ringemann, R. Medda, G. Schwarzmann, K. Sandhoff, S. Polyakova, V.N. Belov, B. Hein, C. von Middendorff, A. Schönle, S.W. Hell, Direct observation of the nanoscale dynamics of membrane lipids in a living cell, Nature 457 (2009) 1159–1162, https://doi.org/10.1038/nature07596.
[26] F.R. Moss, S.G. Boxer, Atomic recombination in dynamic secondary ion mass spectrometry probes distance in lipid assemblies: a nanometer chemical ruler, J. Am. Chem. Soc. 138 (2016) 16737–16744, https://doi.org/10.1021/jacs.6b10655.
[27] G.W. Kingsley, P.B. Feigenson, The synthesis of a perdueterated phospholipid: 1,2-dimyristoyl-sn-glycero-3-phosphocholine-d72, Chem. Phys. Lipids 24 (1979) 135–147.
[28] J.T. Buboltz, G.W. Feigenson, A novel strategy for the preparation of liposomes: rapid solvent exchange, Biochim. Biophys. Acta Biomembr. 1417 (1999) 232–245, https://doi.org/10.1016/S0005-2736(99)00006-1.
[29] M.I. Angelova, D.S. Dimitrov, Liposome electroformation, Faraday Discuss. Chem. Soc. 81 (1986) 303, https://doi.org/10.1039/dc9868100303.
[30] C. Esposito, A. Tian, S. Melamed, C. Johnson, S.-Y. Tee, T. Baumgart, Flicker spectroscopy of thermal lipid bilayer domain boundary fluctuations, Biophys. J. 93 (2007) 3169–3181, https://doi.org/10.1529/biophysj.107.111922.
[31] T.M. Konyakhina, J. Wu, J.D. Mastroianni, F.A. Heberle, G.W. Feigenson, Phase diagram of a 4-component lipid mixture: DSPC/DOPC/POPC/chol, Biochim. Biophys. Acta Biomembr. 1828 (2013) 2204–2214, https://doi.org/10.1016/j.bbamem.2013.05.020.
[32] F. Nelson, J. Wu Morales-Penningston, E.R. Farkas, S.L. Goh, T.M. Konyakhina, J. Y. Zheng, W.W. Webb, G.W. Feigenson, GUV preparation and imaging: minimizing artifacts, Biochim. Biophys. Acta 1798 (2010) 1324–1332, https://doi.org/10.1016/j.bbamem.2010.03.011.
[33] B.A. Camley, C. Esposito, T. Baumgart, F.L.H. Brown, Lipid bilayer domain fluctuations as a probe of membrane viscosity, Biophys. J. 99 (2010) L44–L46, https://doi.org/10.1016/j.bpj.2010.07.007.
[34] R.J. Ryham, T.S. Klotz, L. Yao, F.S. Cohen, Calculating transition energy barriers and characterizing activation states for steps of fusion, Biophys. J. 110 (2016) 1110–1124, https://doi.org/10.1016/j.bpj.2016.01.013.
[35] J.M. Warner, B. O'Shaughnessy, The hemifused state on the pathway to membrane fusion, Phys. Rev. Lett. 108 (2012), https://doi.org/10.1103/PhysRevLett.108.178101.
[36] S.T. Yang, V. Kiessling, L.K. Tamm, Line tension at lipid phase boundaries as driving force for HIV fusion peptide-mediated fusion, Nat. Commun. 7 (2016), 11401, https://doi.org/10.1038/ncomms11401.
[37] X. Banquy, K. Kristiansen, D.W. Lee, J.N. Israelachvili, Adhesion and hemifusion of cytoplasmic myelin lipid membranes are highly dependent on the lipid composition, Biochim. Biophys. Acta Biomembr. 1818 (2012) 402–410, https://doi.org/10.1016/j.bbamem.2011.10.015.
[38] D.W. Lee, K. Kristiansen, S.H. Donaldson, N. Cadirov, X. Banquy, J.N. Israelachvili, Real-time intermembrane force measurements and imaging of lipid domain morphology during hemifusion, Nat. Commun. 6 (2015), 7238, https://doi.org/10.1038/ncomms8238.
[39] D. Marquardt, F.A. Heberle, T. Miti, B. Eicher, E. London, J. Katsaras, G. Pabst, 1H NMR shows slow phospholipid flip-flop in gel and fluid bilayers, Langmuir 33 (2017) 3731–3741, https://doi.org/10.1021/acs.langmuir.6b04485.
[40] M. Doktorova, F.A. Heberle, B. Eicher, R.F. Standaert, J. Katsaras, E. London, G. Pabst, D. Marquardt, Preparation of asymmetric phospholipid vesicles for use as cell membrane models, Nat. Protoc. 13 (2018) 2086–2101, https://doi.org/10.1038/s41596-018-0033-6.
[41] R.J. Bruckner, S.S. Mansy, A. Ricardo, L. Mahadevan, J.W. Szostak, Flip-flop-induced relaxation of bending energy: implications for membrane remodeling, Biophys. J. 97 (2009) 3113–3122, https://doi.org/10.1016/j.bpj.2009.09.025.
[42] T.L. Steck, J. Ye, Y. Lange, Probing red cell membrane cholesterol movement with cyclodextrin, Biophys. J. 83 (2002) 2118–2125, https://doi.org/10.1016/S0006-3495(02)73972-6.
[43] R. Leventis, J.R. Silvius, Use of cyclodextrins to monitor transbilayer movement and differential lipid affinities of cholesterol, Biophys. J. 81 (2001) 2257–2267, https://doi.org/10.1016/S0006-3495(01)75873-0.
[44] A. Hossein, M. Deserno, Spontaneous curvature, differential stress, and bending modulus of asymmetric lipid membranes, Biophys. J. 118 (2020) 624–642, https://doi.org/10.1016/j.bpj.2019.11.3398.
[45] D.W. Allender, A.J. Sodt, M. Schick, Cholesterol-dependent bending energy is important in cholesterol distribution of the plasma membrane, Biophys. J. 116 (2019) 2356–2366, https://doi.org/10.1016/j.bpj.2019.03.028.
[46] J. Huang, S. Hiraki, G.W. Feigenson, Calculation of liquid-disordered/liquid-ordered line tension from pairwise lipid interactions, J. Phys. Chem. B 124 (2020) 4949–4959, https://doi.org/10.1021/acs.jpcb.0c03329.
[47] S. Seo, M. Murata, W. Shinoda, Pivotal role of interdigitation in interleaflet interactions: implications from molecular dynamics simulations, J. Phys. Chem. Lett. 11 (2020) 5171–5176, https://doi.org/10.1021/acs.jpclett.0c01317.
[48] J.D. Perlmutter, J.N. Sachs, Interleaflet interaction and asymmetry in phase separated lipid bilayers: molecular dynamics simulations, J. Am. Chem. Soc. 133 (2011) 6563–6577, https://doi.org/10.1021/ja106626r.
[49] M.D. Collins, Interleaflet coupling mechanisms in bilayers of lipids and cholesterol, Biophys. J. 94 (2008) L32–L34, https://doi.org/10.1529/biophysj.107.124362.
[50] G.G. Putzel, M.J. Uline, I. Szleifer, M. Schick, Interleaflet coupling and domain registry in phase-separated lipid bilayers, Biophys. J. 100 (2011) 996–1004, https://doi.org/10.1016/j.bpj.2011.01.021.
[51] H.J. Risselad, S.J. Marrink, The molecular face of lipid rafts in model membranes, Proc. Natl. Acad. Sci. U. S. A. 105 (2008) 17367–17372, https://doi.org/10.1073/pnas.0807527105.